CONTACT ANALYSIS OF HEAVY-DUTY APRON FEEDER WITH CLEARANCE

Jiahui Peng[1*] – Xiangwen Cheng[1] – Jia Wang[2] – Lichun Xiao[2]

[1] College of Mechanical Engineering, North China University of Science and Technology, Hebei Tangshan 063210, China
[2] Tangshan Tianhe Environmental Protection Technology Co, ltd., Hebei Province Mineral Classification Crushing Equipment Technology Innovation Center, Tangshan 063000, China

ARTICLE INFO

***Article history*:**
Received: 16.04.2023.
Received in revised form: 07.07.2023.
Accepted: 16.07.2023.

Keywords:

Heavy-duty Apron Feeder
Clearance structure
Nonlinear contact
Impact load
Finite element

DOI: https://doi.org/10.30765/er.2229:

Abstract:

The problem of clearance contact between the bearing plate and the supporting guide rail is studied when the heavy-duty Apron Feeder is subjected to impact load. Based on the energy method, the impact force of the falling ore was calculated, and the nonlinear contact finite element analysis of the structure with clearance was performed using ANSYS Workbench. The results show that at the first moment of contact, the initial contact shape is an approximately linear contact, and then a deformation occurs near the contact line, which quickly evolves from a linear contact to a surface contact. The contact stress distribution is diffused outward along the initial contact boundary and gradually decreases, and the stress concentration occurs at the contact boundary. When the distance is different, the shape of the contact area is similar, but when the distance is large, the contact area is small and the stress distribution is more concentrated. The nonlinear contact calculation of the skirt feeder reveals the instantaneous contact process of the plate rail under the impact force and determines the influence of the distance size on the contact properties, which provides a theoretical basis for the selection of the distance value.

1 Introduction

The heavy-duty apron feeder is an important transportation equipment for mining [1]. The supporting part of the feeder is mainly composed of the bearing plate, chain, guide rail and support wheel [2], as shown in Figure 1. The driving device outputs energy to drive the rotation of the sprocket, the teeth of the sprocket engage with the chain pin and pull the chain to perform continuous motion [3]. The support wheel has the function of supporting the chain to ensure the stability of the bearing plate during operation. At the same time, the flange of the roller can limit the deviation of the chain. The bearing plate is attached to the chain with pins, and the chain drives the bearing plate to move synchronously, which finally fulfils the purpose of ore transportation [4]. The guide rail is attached to the main frame with bolts to support the bearing plate. When the conveyor runs stably, a clearance between the bearing plate and the supporting guide rail is required to avoid the continuous sliding friction between the moving bearing plate and the supporting guide rail. But when the feeder is affected by the impact force caused by the fall of large ores, the bearing plate will produce a large deformation, so that the clearance is closed, at this time, the supporting guide rail and the bearing plate are in contact, the two jointly bear the impact load, the deformation and tension of the bearing plate is limited in a certain range.

It can be seen that the bearing plate and supporting guide rail form a contact pair with clearance when the conveyor is subjected to impact load. The nonlinear dynamic characteristics caused by the contact [5] make

* Corresponding author
E-mail address: cxw@ncst.edu.cn

the mechanical response of the supporting part of the conveyor after the impact load extremely complex, and the magnitude of the clearance value also has a significant influence on the contact state of the structure [6].

1.Bearing plate; 2.Plate and rail contact position; 3.Support guide rail; 4.Traction chain; 5.Support wheel

Figure 1. Bearing part of heavy-duty apron feeder

The design and selection of the apron feeder is usually calculated using a combination of general design manual, calculation standards and finite element simulation. The design manual and calculation standards rarely take into account the actual working environment and various loading conditions of the equipment, and there is no differentiated design and improvement between different types of apron feeders. Benefiting from the rapid development of computer power and gradually mature simulation software, the finite element method of elastic mechanics is used for the design of important structures, which can more realistically simulate the complex structure of the machine and various operating conditions, so that in recent years, the proportion of engineering applications is becoming higher and higher.

Chen [7] studied the restrictive relationship between the loading width, height and tilt Angle of the feeder, established the differential equation and deduced the theoretical formula among the three, which provided a theoretical basis for the design of the loading limit height and tilt Angle of the heavy apron feeder. Wan [8] et al. calculated the effective design height of the apron board based on granular mechanics, and gave the material flow pattern related to the speed and height of the apron board, providing a design reference for the chute and apron board. According to the main technical parameters of the feeder, He [9] et al. gave the calculation methods of total operating resistance, bunker pressure and driving power through theoretical and empirical formulas, and selected the key parts of the feeder reasonably and economically according to the calculation data. Ying [10] calculated various loads on the feeder, used ANSYS finite element software to calculate the strength and stiffness of the feeder frame, and improved the structure according to the calculated results. Qu [11] et al. carried out static and modal analysis on the frame of the apron feeder, and obtained the stress concentration position of the frame and the natural frequency and vibration mode of the first 6 modes. Yuan [12] created a virtual prototype of the apron feeder based on RecurDyn, simulated the dynamic power of the apron feeder during no-load/full-load start-up, stable running and braking, and checked the static strength and stiffness of key components by using finite element method.

In summary, many scholars have analyzed and calculated the design selection and static and dynamic analysis of the apron feeder, but they all stay in the study of the key components or the overall structure. At present, the influence of the non-entity structure of the slate-rail clearance on the bearing contact characteristics of the equipment is still in the blank stage of research. The selection method of the clearance value is mainly based on empirical data, and the consideration factors are not comprehensive and lack of theoretical basis.

The question of whether the value of the clearance is appropriate greatly affects the bearing capacity and smooth operation of the conveyor, which is the main problem in the structural design of the conveyor. In this paper, in order to avoid the failure of the bearing plate and the guide rail caused by an unreasonable value of the bearing clearance, a nonlinear contact dynamics simulation analysis of the bearing with clearance is carried out, and the contact shape between the bearing plate and the guide rail is studied when the bearing is subjected to the impact load of the falling ore. The influence of the size of the clearance on the contact characteristics of the plate and rail is analyzed, the most unfavorable operating conditions are determined, and it is checked whether the conveyor can operate normally under these operating conditions. The purpose of this study is to

show the real contact between the bearing plate and the guide rail, to provide a theoretical basis for the selection of the clearance value, and to give guidance for the design and improvement of the heavy apron feeder.

2 Contact characteristics and research scheme

According to the relative size of the contact area, the contact phenomena can be divided into two categories: conformal contact and non-conformal contact. Non-conformal contact means that the two contacts are initially point contact or line contact, and gradually produce a "contact area" during the loading process, and the contact area is small relative to the size of the two contact objects. In this case, the contact area produces a local stress concentration, as shown in Figure 2(a). Conformal contact refers to the contact situation where the size of the contact area and the curvature radius of the contact area of the object are approximately equal, and there is no obvious contact area. For example, washer fitting, punch punching, and pressure processing are conformal contact types, as shown in Figure 2(b).

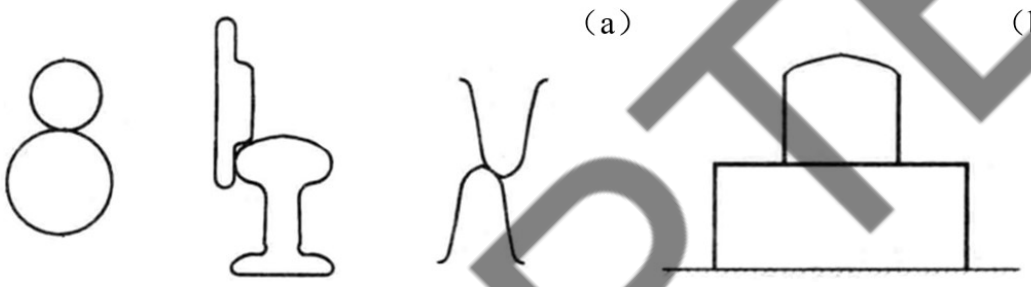

(a) non-conformal contact; (b) conformal contact

Figure 2. Contact type

The position of contact between the bearing plate and the support guide rail is two planes, and the larger contact area belongs to conformal contact. The shape and size of the contact area will change with the difference of the clearance, and the contact area can not be accurately distinguished. The Hertz contact model based on the elastic half-space theory assumes that the width of the contact area is far less than the curvature radius of the contact point, so it has a high accuracy only when solving the non-conformal contact problem [13]. However, when solving the conformal contact problem, the calculated contact stiffness is too small, and the adoption of this kind of point contact model to solve the plate rail contact problem may cause large errors. In addition, in the process of contact between the bearing plate and the guide rail, due to the existence of clearance, it is unknown whether the two surfaces contact each other or separate. The contact state may have sudden changes, and the influence of friction should be considered in the analysis of the contact process, so the Hertz hypothesis is no longer applicable.

There is no theoretical solution to the non-Hertzian contact problem for large contact areas. Since the length of the two contact areas is different, stress concentration occurs at the contact boundary [14]. Therefore, a numerical method is applied in this work to solve this problem. Using the finite element analysis of ANSYS Workbench, the contact area is first divided into small units, and the underlying contact deformation is calculated by numerical integration. It can avoid the assumption of elastic half-space in classical contact theory, accurately simulate the geometric shape of the bearing plate and supporting guide rail and their contact relationship, and effectively solve many complex nonlinear contact problems [15]. Finite element simulation analysis of contact dynamics with clearance was carried out on the bearing part of the feeder to explore the instantaneous contact collision behavior of the bearing plate and supporting guide under the impact load condition, and the influence of the backlash value on the contact characteristics of the bearing plate and supporting guide was analyzed.

3 Theoretical calculation of impact load

During the operation of the heavy-duty apron feeder, it is temporarily affected by the impact load caused by the fall of large ores. Such a pulsating impact with a large range of fluctuation in a very short time [16] causes a strong deformation of the supporting plate and a violent contact and collision with the supporting guide rail. Therefore, it is necessary to calculate the impact force of the falling ore, load the finite element

model and analyze the contact collision behavior between the bearing plate and the supporting guide rail under the impact.

Because of the complexity of the impact problem, it is difficult to solve it accurately. Therefore, in engineering, the energy method is often used to solve the impact problem and calculate the impact force of ore falling. In the process of impact, the ore with mass *m* falls and the bearing plate will adhere to each other and move together once they contact. When the deformation of the bearing plate reaches the maximum position, the speed of the system becomes zero and the deformation of the bearing plate is Δ_d, then the potential energy variation of the ore in the impact process is

$$\Delta V = mg\Delta_d \tag{1}$$

The kinetic energy ΔT and potential energy ΔV of the impact system are all converted into the deformation energy $V_{\varepsilon d}$ of the bearing plate.

$$V_{\varepsilon d} = \Delta T + \Delta V \tag{2}$$

When the velocity of the system is zero, the dynamic load F_d acting on the bearing plate is the maximum value and is proportional to the variation of the bearing plate. Therefore, the work done by the dynamic load in the impact process is the deformation energy of the bearing plate:

$$V_{\varepsilon d} = \frac{1}{2} F_d \Delta_d \tag{3}$$

Assume that the ore of mass *m* acts on the bearing plate in static load mode, and the static deformation and stress distribution of the bearing plate are Δ_{st} and σ_{st}. In the online elastic range, static load and static deformation are directly proportional to dynamic load and dynamic variation, so:

$$\frac{F_d}{mg} = \frac{\Delta_d}{\Delta_{st}} = \frac{\sigma_d}{\sigma_{st}} \tag{4}$$

$$\begin{cases} F_d = \dfrac{\Delta_d}{\Delta_{st}} mg \\ \sigma_d = \dfrac{\Delta_d}{\Delta_{st}} \sigma_{st} \end{cases} \tag{5}$$

Substituting F_d in equation (5) into equation (3) can be obtained

$$V_{\varepsilon d} = \frac{1}{2} \frac{\Delta_d^{\,2}}{\Delta_{st}} mg \tag{6}$$

Equation (6) and (1) are put into equation (2), and after finishing, the mobilization deformation Δ_d and impact dynamic load coefficient K_d are obtained:

$$\Delta_d = \Delta_{st}\left(1 + \sqrt{1 + \frac{2\Delta T}{mg\Delta_{st}}}\right) \tag{7}$$

$$K_d = \frac{\Delta_d}{\Delta_{st}} = 1 + \sqrt{1 + \frac{2\Delta T}{mg\Delta_{st}}} \tag{8}$$

The impact load is formed by the material falling freely from a height, and the velocity and kinetic energy when the material contacts the bearing plate are:

$$v = \sqrt{2gh} \tag{9}$$

$$\Delta T = \frac{1}{2} mv^2 = mgh \tag{10}$$

It can be calculated by substituting the ore kinetic energy ΔT into the impact dynamic load coefficient K_d

$$K_d = 1 + \sqrt{1 + \frac{2h}{\Delta_{st}}} \tag{11}$$

According to the parameters in Table 1, the maximum particle size of the ore calculated by finite element method can make the bearing plate produce a static deformation of 6.312×10^{-4}m, and the falling height is 1m. By putting the data into equation (11), the impact load coefficient is calculated to be about 57.3. When the ore directly impacts the bearing plate, the maximum impact load is calculated

$$F_{max} = K_d mg = 970341\text{N} \tag{12}$$

But in the actual work, large ore can not directly impact bearing plate, apron feeder operation specifications clearly indicated that the need to put small ore on the bearing plate as protection, under normal circumstances is not allowed to discharge, so there is a small ore as a buffer layer makes the impact force is much smaller than the large ore direct impact bearing plate. When the bearing plate is empty, the impact force of the large ore directly on the bearing plate is enough to deform or even break the bearing plate, chain and support wheel. Therefore, the role of the buffer layer should be considered when calculating the impact force. The buffer layer consists of discontinuous media with complex shape and structure, which cannot be solved accurately by the finite element method or theoretical calculations. The stone impact test [17] is used to calculate the stone impact force after penetrating the buffer layer, and its accuracy is verified by comparison with the measured value. The effective impact force formed at the bottom of the buffer layer by the stone impact force penetrating the buffer layer:

$$P = \frac{3F_{\max}(1 - \cos\theta)}{4L} \tag{13}$$

Where, P is impact force Effective impact force acting on the bottom through the buffer layer; $F_{\max}$ is the maximum impact force; L is Buffer thickness; θ is the diffusion Angle of rockfall impact force is taken as the passive rupture Angle: $45° - \varphi/2$; φ is internal friction Angle of buffer layer.

According to the internal friction Angle of lignite bulk in Table 1, which is 37° [18], the diffusion Angle is calculated to be 26.5°, and the thickness of buffer layer is substituted into equation (13), so that the effective impact force of falling ore with the maximum particle size on the bearing plate is about 76462N.

Table 1. Parameters of ore.

Description	Parameters
Transported ore	lignite
Density	1200kg/m^3
The maximum particle size of the ore transported	1200×1000×1000mm
Angle of internal friction of lignite particles	37°
Buffer thickness	1000mm

4 Establish finite element model

When the feeder is affected by the free fall of the ore, there are two paths to transfer the impact to the main frame, as shown in Figure 3:

1) The impact force is transmitted to the chain and the support wheel through the bearing plate, and finally to the main frame through the bearing seat of the support wheel;

2) The bearing plate deforms after being stressed, and the impact is transmitted to the main frame through contact with the support guide rail fixed on the main frame.

In the second path, the plate and rail will form a violent contact collision. If the contact stress is too large, the bearing plate or the support guide will produce plastic deformation, resulting in the loss of the support guide's bearing capacity. If the impact force cannot be transferred to the main frame through path 2, the bearing plate, chain and support wheel will bear too much load. At this time the apron feeder will not immediately lose carrying capacity, difficult to detect the first time in the occurrence of failure. Once the guide rail fails and works for a long time, the bearing part will be damaged, which will seriously affect the production efficiency of the equipment and cause significant economic losses. Therefore, it is necessary to establish the finite element model of the bearing part of the apron feeder, and analyze the contact collision behavior with clearance between the bearing plate and the supporting guide rail under the impact load.

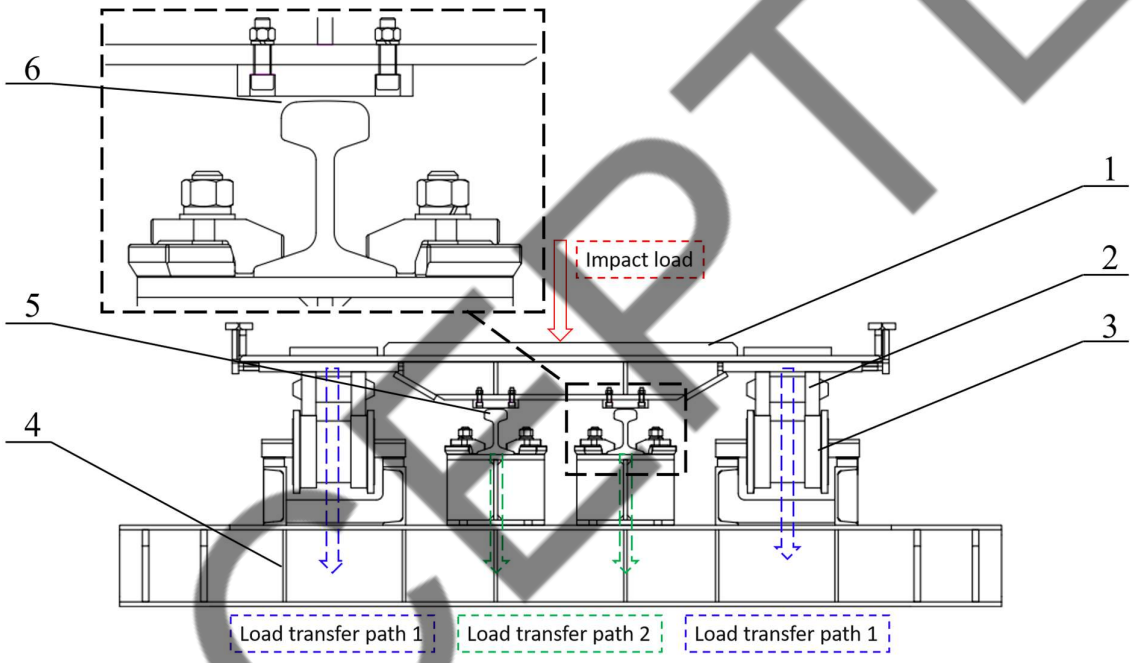

1.Bearing plate; 2.Chain; 3.Support wheel; 4.Main frame; 5.Support guide rail; 6.Plate-rail clearance

Figure 3. Stress situation of bearing part

4.1 Build 3D solid model

According to the assembly drawing of the bearing part of the heavy-duty apron feeder shown in Figure 3, solid modeling was carried out on the four key bearing parts, namely, the bearing plate, chain, support guide rail, support wheel and its bearing seat, in the Creo 3D modeling software, ignoring the main frame and making necessary reasonable simplification of the parts. Each bearing plate carries the ore above it independently and is not affected by the other bearing plates. Therefore, when finite element analysis is carried out on the bearing part, a single bearing plate can be modeled and simulated. Three link of the chain between two support wheels were established as a simplified model to replace the whole chain. The solid model is shown in Figure 4.

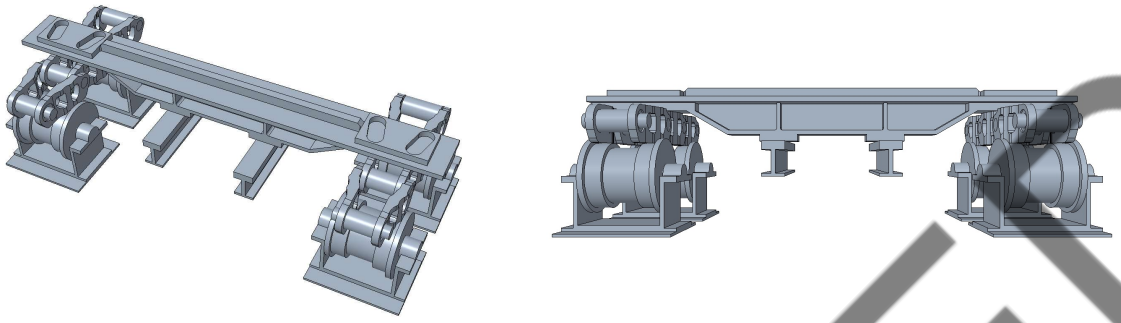

Figure 4. 3D Solid model of bearing part of apron feeder

4.2 Material properties and cell meshing

The bearing plate is made of low-alloy high-strength steel Q355-D, and the supporting guide rail is made of Q550. The material properties are shown in Table 2, and the mechanical properties of materials are shown in Table 3

Table 2. Material property.

Material name	density, kg/m3	Modulus of elasticity, MPa	Poisson's ratio
Q355-D	7850	2.06×10^5	0.3
Q550	7850	2.06×10^5	0.3

Table 3. Mechanical properties of materials.

Thickness or diameter of steel, mm	Yield strength, MPa	
	Q355-D	Q550
t≤16	355	550
16 < t≤40	345	540
40 < t≤63	335	530
63 < t≤80	325	520

The model was imported into ANSYS Workbench for finite element preprocessing, using high level solid elements and tetrahedral meshing. The mesh of the contact position is encrypted, and "contact size" is inserted in the contact area of the plate and rail, and a unit is created on the contact surface of the geometry, so that the contact area has a similar encrypted size. The total number of elements in the final finite element model is 403830 and the total number of nodes is 667394, as shown in Figure 5.

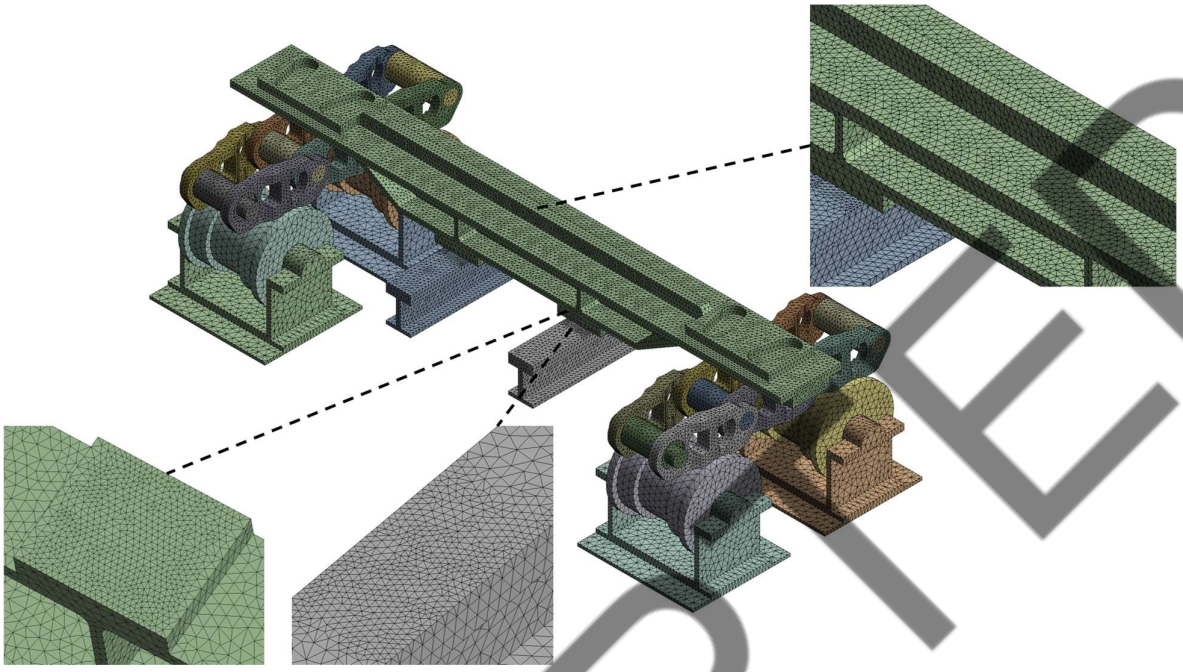

Figure 5. Finite element model of bearing part

4.3 Boundary condition

According to the actual working condition of the traction chain, the translational freedom of Z direction and the rotational freedom of X and Y direction between the pin shaft and the chain plate shaft hole were constrained. The bearing seat of the support wheel restrains the support wheel through the sliding bearing, so the translational freedom in the Z direction and the rotational freedom in the X and Y directions between the support wheel and the support wheel need to be restrained. Table 4 shows the specific constraint relationship between the chain pin shaft and the chain piece shaft hole, and Table 5 shows the constraint relationship between the axle hole of the support wheel and the support shaft. The geometric view of the constraint relationship between the two is shown in Figure 6.

Table 4. Chain pin and hole constraint relationship.

Constraint form	Translational constraint	Rotation constraint
Constraint direction	Z direction	X and Y direction

Table 5. Constraint relationship between support wheel and bearing seat.

Constraint form	Translational constraint	Rotation constraint
Constraint direction	Z direction	X and Y direction

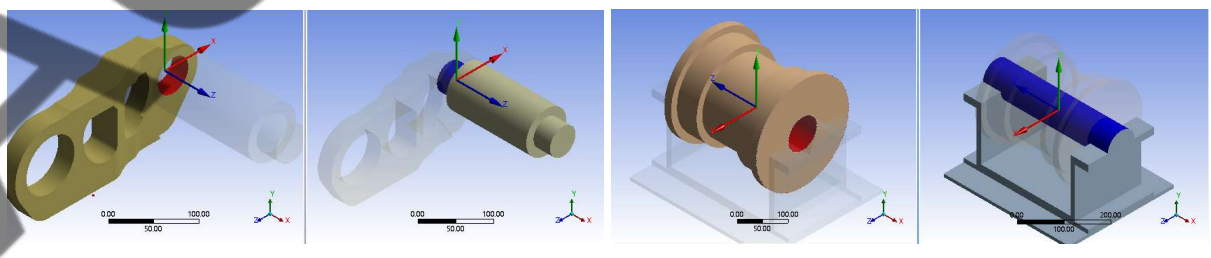

(a) Chain pin and shaft hole *(b) Support wheel shaft hole and bearing seat*

Figure 6. Constraint relationship geometry view.

In the actual structure, the support rail and the support wheel bearing seat are attached to the main frame, and the bearing plate is connected to the chain by pins. When the longitudinal displacement generated by the bearing plate during the loading process exceeds the clearance value, frictional contact with the support guide rail occurs. The overall constraint position and the settings of the contact pairs are shown in Table 6. The contact position between the bearing plate and the supporting guide rail is shown in Figure 7, where the upper surface of the guide rail is set as the contact surface and the contact position of the bearing plate is set as the target surface. The running resistance of the feeder in the running process causes the tensile chain to generate tension, exert a tensile load on the three established chains, and finally exert an impact load by the ore falling on the surface of the bearing plate. For the finite element analysis, models with 1 mm, 1.5 mm and 2 mm clearance were created to analyze the influence of the clearance on the contact properties between the bearing plate and the supporting guide rail.

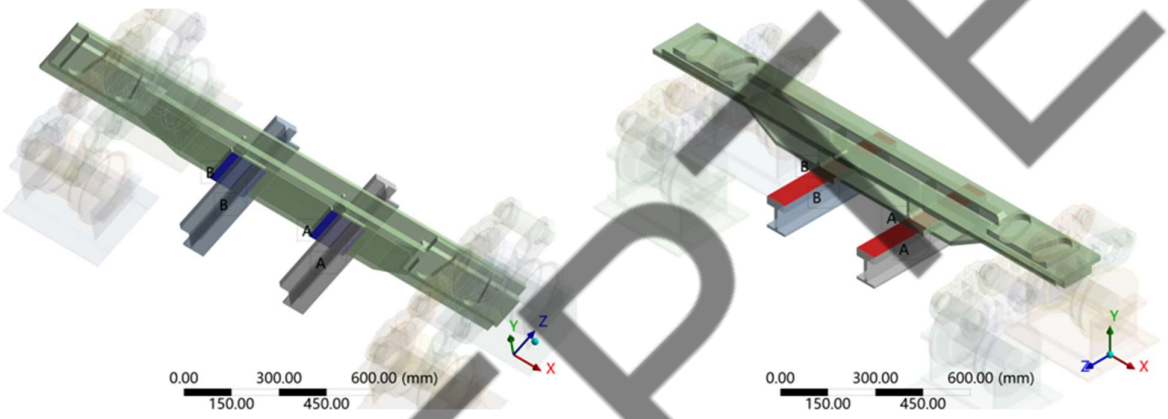

(a) Target surface *(b) Contact surface*

Figure 7. The contact setting between the bearing plate and the supporting guide rail.

Table 6. Constraints and contact settings

Applied position	Connection relation
Support the bottom of the guide rail	Fixed Support
Underside of bearing seat of support wheel	Fixed Support
Bearing plate and chain	Bonded
Bearing plate and supporting guide rail	Frictional

5 Results and discussion

After the contact collision between the bearing plate and the supporting guide rail, extrusion deformation and friction occur on the two contact surfaces, especially at the contact boundary, where the stress value is very high and may exceed the yield strength of the material, resulting in unrecoverable plastic deformation [14]. The main cause of surface damage such as wear and flaking of plates and rails is the contact stress between plates and rails. According to the yield criterion of materials in the fourth strength theory, plastic deformation occurs when the contact stress exceeds the yield strength limit of materials [15]. To ensure that parts do not fail due to contact stress, the change in contact properties with clearance must be analyzed. The sliding friction generated by the sheet metal rail after contact causes the conveyor to generate additional resistance in the transport process, puts additional load on the drive device, and affects the smooth operation of the conveyor. Therefore, it is necessary to analyze the frictional properties of the plate and rail to ensure that the drive device is not overloaded by the additional resistance caused by the plate and rail contact.

5.1 Contact process and characteristics analysis

In order to directly reflect the contact process between the bearing plate and the supporting guide rail, the stress nephogram of the contact position of the plate and rail was extracted. Figure 8 shows the change of

contact stress distribution in the process of the first contact between the plate and rail. It can be observed from the figure that, at the moment of contact between the bearing plate and the supporting guide rail, the initial contact form is approximately linear contact, and then deformation occurs near the initial contact line under the impact load, which rapidly develops from linear contact to surface contact. As can be seen from Figure 8,the contact area of plate and rail is large, which belongs to conformal contact [19]. The maximum contact stress position appears at the two ends of the contact boundary, and the stress value at the two ends of the boundary is much larger than that in other contact areas.

This is because the bearing plate will bend and deform after being impacted by the falling ore, resulting in a certain Angle between the two contact surfaces of the bearing plate and the guide rail when they contact, which is not completely parallel. At this time, the two contact surfaces will first contact at the inner boundary, and then the contact position will produce a small elastic deformation under the action of the force, so that the contact stress can be diffused outwards. Therefore, in the process of contact between the bearing plate and the guide rail, the stress distribution is spread outward along the inner contact boundary and gradually decreases.

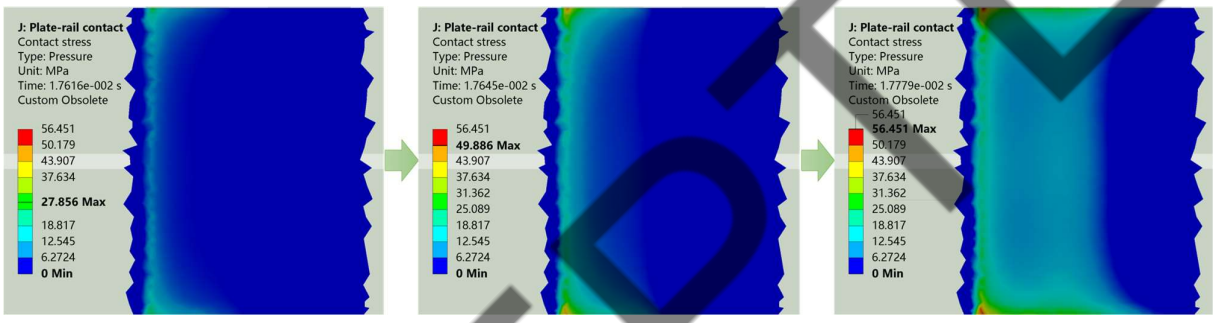

Figure 8. Contact process of plate and rail under impact force

Insert the "path" into the finite element model at the position of the contact boundary of the plate and rail contact surface, as shown in the line from position 1 to 2 in Figure 9. The contact stress distribution on this path is extracted, as shown in Figure 10. It can be observed from the figure that there is a significant increase in stress values at both ends of the contact edge of the plate and rail. Combined with the stress distribution nephogram in Figure 8, it can be seen that stress concentration occurs at both ends of the contact boundary.

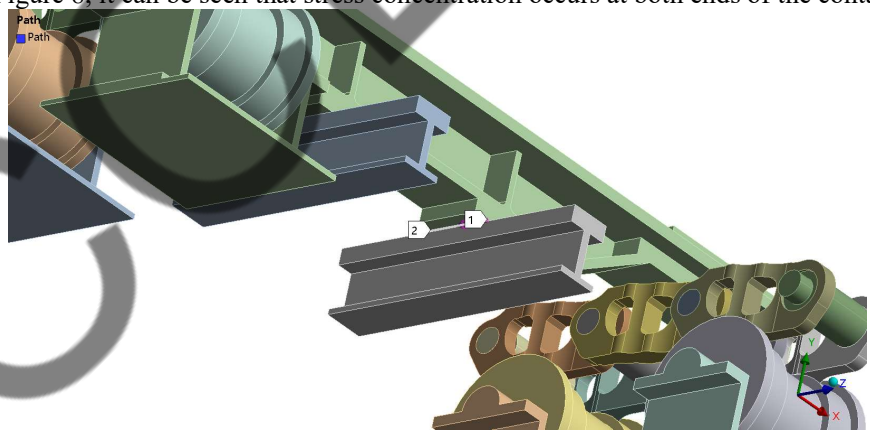

Figure 9. The stress sampling path at the contact boundary

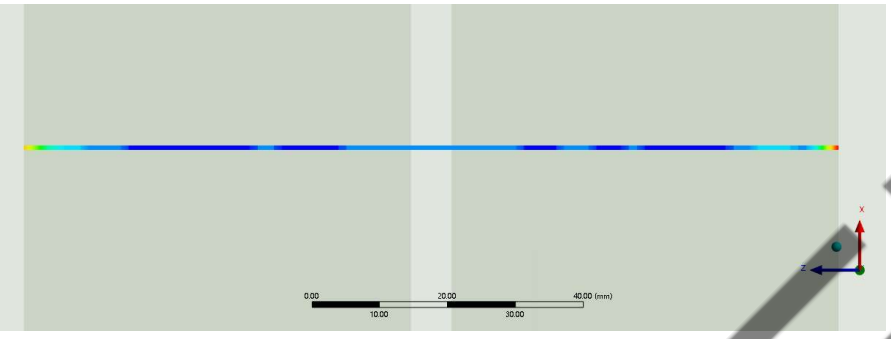

(a) Nephogram of contact stress distribution

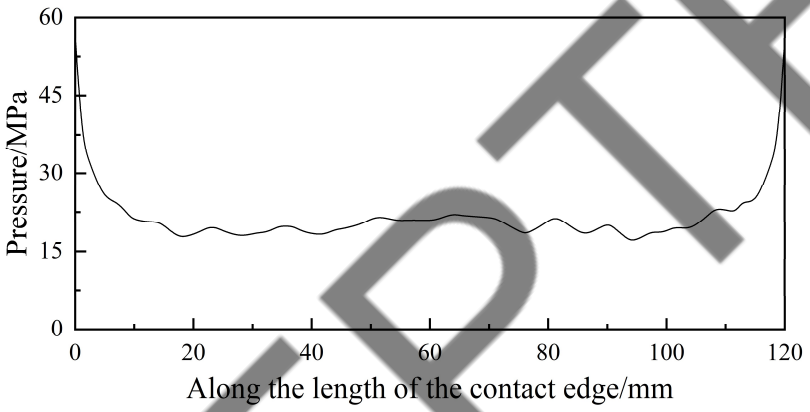

(b) Contact stress distribution curve

Figure 10. The stress sampling path at the contact boundary

5.2 Contact stress analysis at different clearances

Figure 11 shows the contact stress distribution of plate and rail with different clearances. It can be observed from the figure that when the clearance size is different, the contact stress distribution of plate and rail is similar, but the contact area of large clearance is small and the contact stress distribution is more concentrated, while the contact area of small clearance is larger and the contact stress distribution is more uniform.

This is because when the clearance between the plate and rail is large, the bearing plate will undergo significant bending deformation after being impacted by the ore falling, resulting in a smaller overlap ratio of the contact surface between the bearing plate and the guide rail. The plate and rail only produce a smaller contact area at the inner contact boundary line, resulting in a more concentrated stress distribution; When the clearance between the plates and rails is small and the bearing plate has not undergone significant bending deformation, it has already come into contact with the guide rail, at this time, the overlap ratio of the two contacts surface is high, the contact area is large, and the stress distribution is uniform.

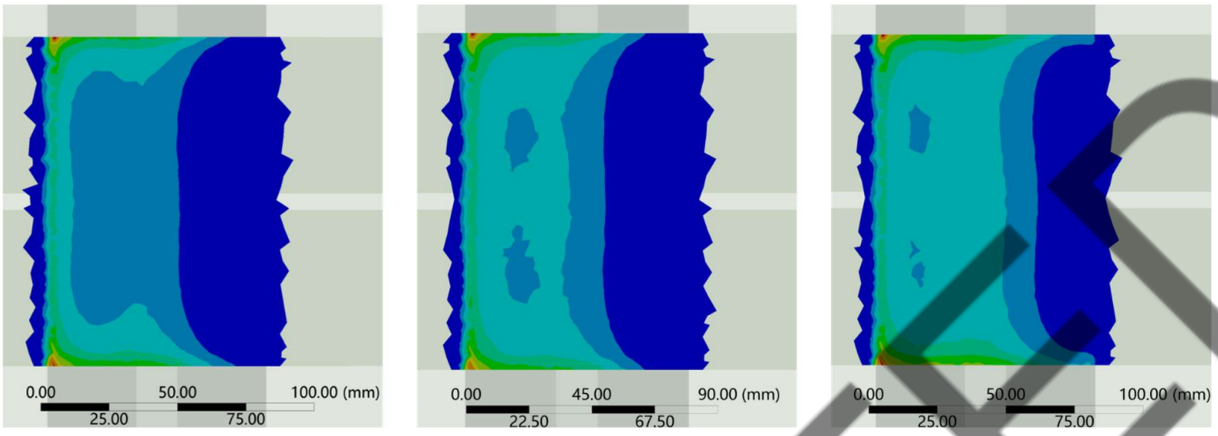

(a) 2mm clearance *(b) 1.5mm clearance* *(c) 1mm clearance*

Figure 11. Contact stress nephogram at different clearances

By solving the normal reaction of the supporting guide rail against the bearing plate in the contact process, the normal dynamic contact force of the plate and the rail is obtained, as shown in Figure 12. It can be seen that the curve of the normal contact force has a strongly nonlinear characteristic and the contact force drops to 0 during the contact. This is due to the presence of the clearance between the plate and rail, so there are only force constraints but no geometric constraints in the collision process. After the initial contact, the plate and the rail enter a "sub-collision phase" [20]. This phase includes multiple minor and minor collisions and multiple separations, a series of multiple collisions that occur in a very short period of time and form a single collision at the macro level [21] until the impact force subsides and the board and rail return to the separation state. The transients during the collision are very obvious, and before the transients of the previous collision are over, the next collision will occur. Therefore, adjacent collisions influence each other, resulting in a highly nonlinear dynamic contact force. Comparing the contact force curves of the three clearance types, we find that when the clearance between the plate and rail is reduced from 2 mm to 1 mm, the peak value of the normal contact force remains approximately the same and the maximum value of the normal contact force of the plate and rail is not significantly affected by the reduction of the clearance.

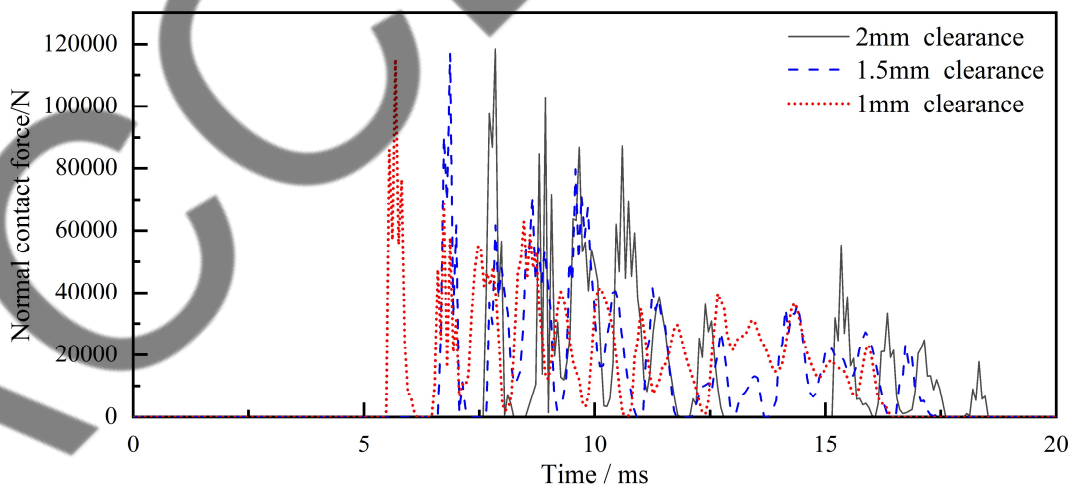

Figure 12. Normal contact force curve of plate and rail with different clearance

The dynamic contact stress curve of plate and rail with three kinds of clearance is shown in Figure 13. By comparing the contact stress curve, it is found that the maximum stress with small clearance is lower than that with large clearance. The maximum contact stress of 2mm clearance is 56.45MPa; The maximum stress of 1.5mm clearance is 46.36MPa; The maximum contact stress of 1mm clearance is 43.10MPa. When the clearance of plate and rail decreased from 2mm to 1mm, the peak contact stress of plate and rail decreased by

23.7%. It can be seen that although the decrease of clearance value has a weak influence on the contact collision force of the plate and rail, it can significantly reduce the contact stress of the plate and rail. According to the analysis based on the contact stress distribution nephogram in Figure 11, when the clearance is smaller, the size of the contact area between the bearing plate and the supporting guide rail is larger, and the contact stress distribution is more uniform. Therefore, the stress concentration phenomenon of the plate and rail at the contact boundary is weakened, so that the peak stress is reduced compared with that in the case of large clearance.

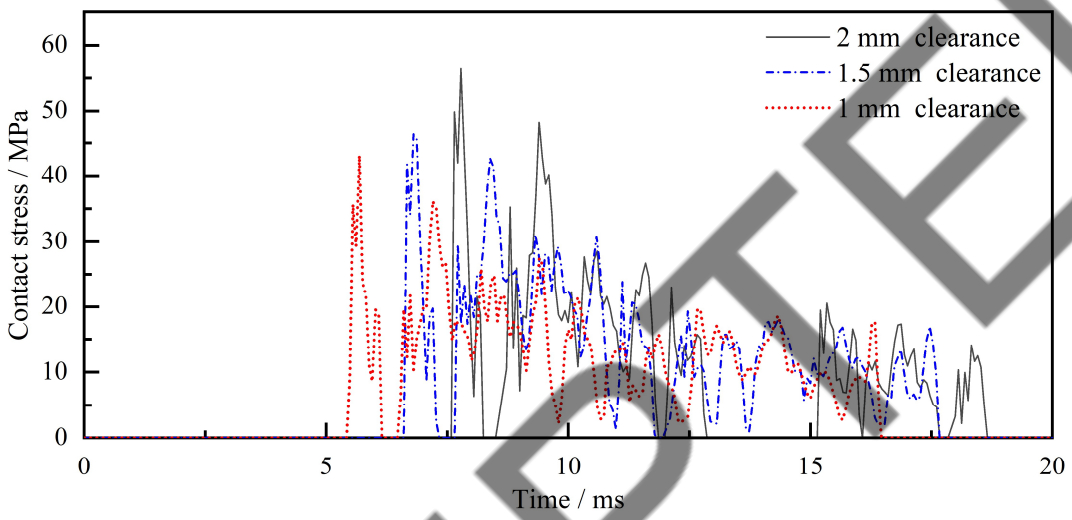

Figure 13. Contact stress curves at different clearances

Through the analysis of the normal contact characteristics of the bearing plate and the supporting guide rail at different clearance, it can be seen that the smaller clearance can significantly reduce the contact stress of the plate and rail, which is conducive to the smooth operation of the feeder and prolong the service life of the apron feeder.

5.3 Analysis of friction characteristics

By solving the tangential reaction given by the guide rail to the bearing plate in the contact process, the friction force of the plate and rail under different clearance structures was obtained, as shown in Figure 13. It can be observed from the figure that the friction force changes dramatically in a very short period of time and then returns to zero. It can be seen that the bearing plate, supported by the tensioning chain, separates from the guide rail immediately after a short contact. The additional resistance generated by the contact between the plate and the rail is intermittent instantaneous friction, and no long-term contact friction will be generated. By comparing the friction curve of the three kinds of clearance, it can be concluded that the peak value of friction decreases with the decrease of clearance. The maximum friction is 12264N at 2mm clearance, 10712N at 1.5mm clearance, and 8851N at 1mm clearance. The friction force decreased by 27.8% when the clearance between plate and rail decreased from 2mm to 1mm.

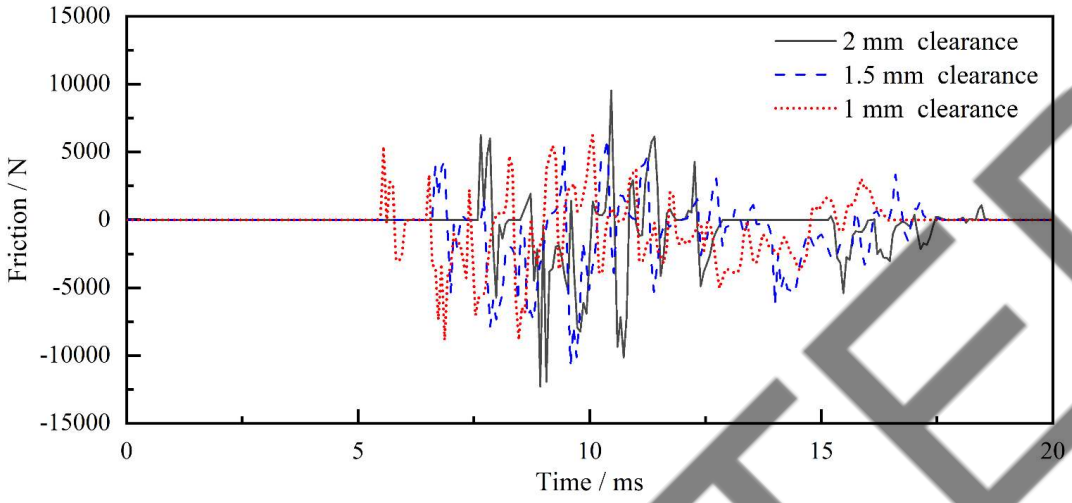

Figure 14. The curve of friction at different clearances

In order to ensure the normal operation of the feeder, it is necessary to calculate the sum of the full load traction F and the maximum additional resistance $F_{\tau\max}$ required by the feeder during transportation, which is less than the maximum driving force provided by the driving device to avoid the overload of the driving device. The rated power of the motor assembled by the apron feeder is 200kW, and the maximum driving force it can provide can be calculated according to equation (14):

$$S_q = \frac{1000 P_e \eta K_0}{v} + S_T' \tag{14}$$

Where, S_q is maximum driving force, N; P_e is Motor rated power, kW; K_0 is Proportional coefficient of motor driving torque to rated torque; η is driving device transmission efficiency; S_T' is drive sprocket winding point tension; v is Chain running speed, m/s.

According to the main data of the apron feeder in Table 7, it can be calculated that the maximum driving force provided by the driving device is 433409N through equation (14). By calculating the running resistance of each section, the final calculation of the feeder under full load required traction is 296755N.

Table 7. Apron feeder main technical parameters

description	parameter
Operating speed	0.53m/s
Rated power of drive motor	200kW
Drive unit transmission efficiency	0.9
Ratio coefficient of motor driving torque to rated torque	1.25

According to equation (15), the sum of the traction force F required by the apron feeder during full load operation and the maximum additional resistance $F_{\tau\max}$ of the contact between the plate and rail is less than the maximum driving force S_q provided by the driving device, and the driving device will not overload due to the additional resistance generated by the contact between the plate and rail.

$$P + F_\tau \le [S_q] \tag{15}$$

When affected by the ore falling, the friction generated by the contact between the plate and rail is instantaneous friction. The additional resistance generated will make the feeder move in the transmission direction, affecting the smooth operation of the apron feeder. The selection of smaller plate rail clearance can reduce the friction caused by this problem, which is conducive to the smooth operation of the feeder.

6 Conclusion

An analysis of the contact dynamics of the supporting part of the heavy apron feeder under the condition of an ore drop impact is carried out, and the influence of the clearance on the contact properties of the structure is studied. The following conclusions are drawn:

(1) After the plate-rail contact, the initial contact shape is a line contact, and then the line contact quickly develops into a surface contact. The stress distribution is diffused outward along the inner contact boundary and gradually decreases, and the stress concentration occurs at the contact boundary of the two contact surfaces.

(2) The value of the clearance has a significant influence on the contact properties. When the clearance is small, the contact area is larger, the stress distribution is more uniform, and the stress concentration phenomenon is weakened, reducing the stress value. The contact friction decreases significantly with the reduction of clearance.

(3) In determining the clearance value, the clearance should be minimized as much as possible to reduce the contact stress and friction, improve the stability of device operation and extend the service life of the device, while ensuring that there is no continuous friction.

In summary, controlling the dynamic contact characteristics of the plate rail of the heavy plate feed bearing through finite element simulation can provide a basis for reducing vibration and noise, improving contact performance, improving bearing capacity, and extending the life of the plate feed bearing under shock loading conditions.

Acknowledgment

This research was supported by the Mineral Classification Crushing Equipment Technology Innovation Center Foundation of Hebei Province (Grant No. SG2021064).

References

[1] T. Thomas, “Expert insights into apron feeder evolution,” The AusIMM Bulletin: Journal of The Australasian Institute of Mining and Metallurgy, no. 4, pp. 55–60, 2019.
[2] J. Z. Huo, S. Q. Yu, and J. Yang, “Structure Optimization Design of Driving Sprocket of Heavy-duty Apron Feeder,” Machinery Design & Manufacture, no. 276, pp. 4–7, 2014.
[3] B. Rajković, Z. Ilić, and R. Rajković, “Driving power verification of the apron feeder for ore transportation,” Mining and Metallurgy Engineering Bor, no. 1-2, pp. 63–70, 2017.
[4] J. Huo, “Static and Dynamic Characteristics of the Chain Drive System of a Heavy Duty Apron Feeder,” The Open Mechanical Engineering Journal, vol. 7, no. 1, pp. 121–128, 2013.
[5] Y. Zhou, Q. Lin, and W. Li, “Optimization of elastoplastic behavior of contact interface for improved contact stress distribution,” Mechanics of Advanced Materials and Structures, no. 4, pp. 803–813, 2023.
[6] S. Suryawanshi, and S. Sundar, “Nonlinear dynamics of system with combined rolling–sliding contact and clearance,” Nonlinear Dynamics, vol. 111, no. 6, pp. 5023-5045, 2022.
[7] L. Z. Chen, “Research on limit inclination angle of heavy apron feeder,” Mining & Processing Equipment, vol. 48, no. 3, pp. 16-20, 2020.
[8] Y. Wan, and L. Z. Chen, “Design of chute and apron of heavy-duty apron feeder,” Mining & Processing Equipment, vol. 47, no. 9, pp. 18-22, 2019.
[9] S. C. He, and Z. F. Lu, “Design and Type Selection Calculation of Heavy Apron Feeder,” Coal Mine Machinery, vol. 38, no. 8, pp. 21-23, 2017.
[10] E. Ying, “Structure Analysis on the Frame of Apron Feeder of Self-mobile Crushing Station,” ed. Dalian University of Technology, Dalian, China, 2017.
[11] Z. Y. Qu, “Structural static and modal analysis of heavy-duty apron feeder based on finite element,” Technology Innovation and Application, no. 19, pp. 28-29, 2022.
[12] X. Y. Yuan, “Dynamic Simulation and Structure Strength Finite Element Analysis of Heavy Apron Feeder,” ed. Jilin University, Jilin, China, 2015.
[13] X. P. Wang, Y. Zhang, and J. Yan, “A contact-impact force model based on variable recovery coefficient,” Journal of Vibration and Shock, vol. 38, no. 5, pp. 198–202, 2019.
[14] X. Q. Huang, “Contact mechanics theory and rolling bearing design analysis,” HUAZHONG University of Science and Technology Publishing Co., Ltd, pp. 36–45, 2018.

[15] J. X. Bian, M. Ning, and Y. Z. Kou, "Finite element analysis of wheel-rail contact of heavy-duty bridge crane under different operating conditions," Modern Manufacturing Engineering, no. 7, pp. 86–92, 2018.
[16] H. J. Sanchez, I. Lombillo, and G. Capellan, "Equivalent Static Force in Heavy Mass Impacts on Structures," International journal of structural stability and dynamics, vol. 22, no. 2, pp. 1–22, 2022.
[17] Y. Zhang, L. Z. Xie, B. He, and P. Zhao, "Research on the Impact Force of Rockfall Impacting Sand Cushions with Different Shapes," Applied Sciences, vol. 12, no. 7, pp. 3540, 2022.
[18] Q. Q. Wu, B. Liu, and Z. Z. Wang, "Numerical Simulation and Experimental Study on the Accumulation Angle of Lignite Particles," Chemical Fertilizer Design, vol. 59, no. 2, pp. 5–8, 2021.
[19] S. Z. Yan, W. K. Xiang, and T. Q. Huang, "Advances in Modeling of Clearance Joints and Dynamics of Mechanical Systems with Clearances," Acta Scientiarum Naturalium Universitatis Pekinensis, vol. 52, no. 4, pp. 741–755, 2016.
[20] X. L. Qi, X. C. Yi, and P. B. Qian, "Experimental Study and Numerical Simulation of Elastic-plastic Sub-impact of Simply Supported Beam Struck by Steel Sphere," Journal of Mechanical Engineering, vol.52, no. 19, pp. 61–72, 2019.
[21] F. Li, and X. L. Qi, "Influence of Mass Ratio on Sub-impact of Flexible Links," Mechanical Science and Technology for Aerospace Engineering, vol.38, no. 8, pp. 1199–1205, 2019.